

Dewetting Transitions in the Self-Assembly of Two Amyloidogenic β -Sheets and the Importance of Matching Surfaces

Zaixing Yang,[†] Biyun Shi,[†] Hangjun Lu,[‡] Peng Xiu,^{*,†} and Ruhong Zhou^{*,§}

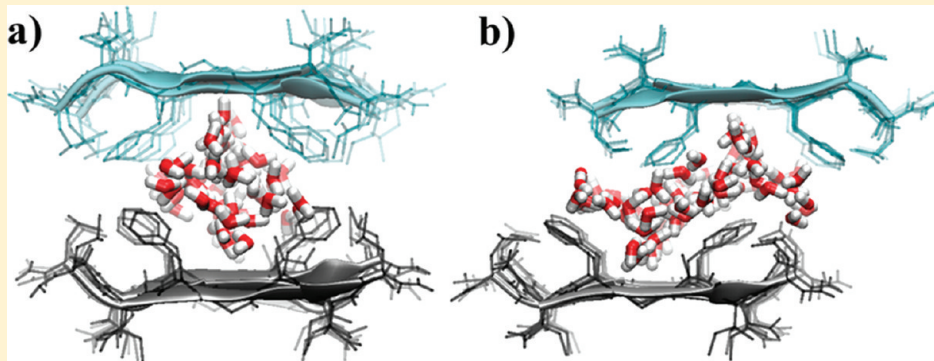
[†]Bio-X Lab, Department of Physics, and Soft Matter Research Center, Zhejiang University, Hangzhou 310027, China

[‡]Department of Physics, Zhejiang Normal University, 321004, Jinhua, China

[§]Computational Biology Center, IBM Thomas J. Watson Research Center, 1101 Kitchawan Road, Yorktown Heights, New York 10598, United States

 Supporting Information

ABSTRACT:



We use molecular dynamics simulations to investigate the water-mediated self-assembly of two amyloidogenic β -sheets of hIAPP_{22–27} peptides (NFGAIL). The initial configurations of β -sheet pairs are packed with two different modes, forming a tube-like nanoscale channel and a slab-like 2-D confinement, respectively. For both packing modes, we observe strong water drying transitions occurring in the intersheet region with high occurrence possibilities, suggesting that the “dewetting transition”-induced collapse may play an important role in promoting the amyloid fibrils formation. However, contrary to general dewetting theory prediction, the slab-like confinement (2-D) shows stronger dewetting phenomenon than the tube-like channel (1-D). This unexpected observation is attributed to the different surface roughness caused by different packing modes. Furthermore, we demonstrated the profound influence of internal surface topology of β -sheet pairs on the dewetting phenomenon through an in silico mutagenesis study. The present study highlights the important role of packing modes (i.e., surface roughness) in the assembly process of β -sheets, which improves our understanding toward the molecular mechanism of the amyloid fibrils formation. In addition, our study also suggests a potential route to regulate controllably the self-assembly process of β -sheets through mutations, which may have future applications in nanotechnology and biotechnology.

INTRODUCTION

Hydrophobic interactions play an important role in many important chemical and biophysical phenomena, such as protein folding, misfolding, and aggregation,^{1–6} ligand binding,^{7–9} self-assembly of amphiphiles,^{10,11} and gating of ion channels.^{12,13} In some extreme cases, the hydrophobic interaction is so strong that there exists a so-called nanoscale dewetting (water drying) transition;^{14–16} that is, when two nanoscale hydrophobic objects (plates) approach each other and reach a critical distance, often large enough to accommodate several layers of water molecules, the water molecules in the interface region are expelled in a very short period of time (~ 100 ps) before the collapse of two plates. The presence and significance of such drying transitions have been investigated in both physical^{15,17–19} and biological

systems.^{5–7,15,20–22} For example, in a previous study, we found a strong water drying transition inside the nanoscale channel (1-D like) formed by the protein melittin tetramer, with a channel size of up to 2 to 3 water diameters.²² There is no dewetting transition found during the two-domain enzyme protein BphC collapse, despite the very strong hydrophobic interfaces between the two domains (2-D like).⁵ These studies indicate that even in the presence of the polar protein backbone a high confinement environment (1-D like), together with sufficiently hydrophobic protein surfaces, can induce a liquid–vapor

Received: May 18, 2011

Revised: August 24, 2011

Published: August 25, 2011

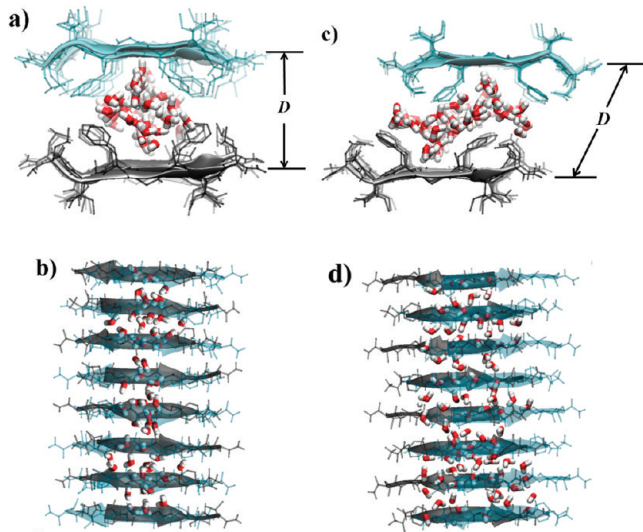


Figure 1. Peptide hIAPP_{22–27} (NFGAIL) model protofilaments, with an initial intersheet separation, $D = 1.2$ nm. Longitudinal and lateral views of initial configurations for the “aligned”-type systems (a,b) and the “staggered”-type systems (c,d). The NFGAIL peptide sheet is shown as ribbons with side chains in sticks, and water is shown as thick bonds. For clarity, only water molecules in the interior of the two sheets are shown. The dark-blue and transparent β -sheets are for the front panel, and the dark-silver and opaque β -sheets are for the back panel.

transition, thus providing an enormous driving force toward further collapse.

It is generally accepted that the higher the confinement for water (such as lower dimensionality), the stronger the dewetting transition. In this study, we will explore the hydrophobic interactions and potential dewetting transitions as well as their controlling factors in the formation of amyloid fibrils. To our surprise, this general rule is challenged by the findings we observe in the self-assembly of two amyloidogenic β -sheets of hIAPP_{22–27} peptides (NFGAIL),^{23,24} which is the subject of our current study.

As we know, many fatal diseases, such as Alzheimer’s disease and type II diabetes, are associated with the presence of amyloid fibrils.^{25–33} It is noteworthy that although the occurrence of amyloid fibrils usually causes diseases, it has been discovered that several natural fibrils have positive functions on the survival of organisms.³⁴ In addition, amyloid fibrils have a unique nanotopography and many advantageous properties and hence are promising candidates for various technological applications,^{34–37} including serving as tools for probing cell behaviors,³⁴ as structural templates for constructing nanowires,³⁵ and as scaffold to organize nanocrystals for use in the electronic industry.³⁷ The basic building blocks of amyloid fibrils are protofilaments, which consist of two or more layers of β -sheets and adopt cross- β -spines with the internal-facing side chains of the adjacent β -sheets fully interdigitated to create a dry interface.^{23,24,38–42} It is of great importance in understanding the protofilaments growth process as well as the physical mechanism behind it. In general, protofilaments grow in two manners: (i) along the fibrillar axis monomer longitudinally patching to the β -sheets⁴³ and (ii) multiple separated β -sheets perpendicular to the fibrillar axis laterally stacking to the protofilament.^{44,45} (See Figure 1.) Recently, Krone et al.²¹ performed molecular dynamics (MD) simulations to study water-mediated assembly of two parallel β -sheets of Alzheimer amyloid- β ($A\beta$) 16–22 peptides (KLVFFAE)

and observed a dewetting transition in which water expulsion precedes hydrophobic collapse for some but not all MD trajectories. This dewetting transition provided the driving force for the collapse of β -sheets. They also suggested that protofilament assembly can be driven by direct interactions between the hydrophobic side chains of the peptides (particularly between F–F residues). By comparison, Reddy et al. found that the assembly of β -sheets formed by the polar heptapeptides (GNNQQNY) from the yeast prion Sup35 was mediated by long-lived structures containing water wires, whereas in the case of the assembly of β -sheets formed by predominantly hydrophobic peptides (GGVVIA) from $A\beta_{37–42}$ peptides, fibril formation and expulsion of water molecules occurred nearly simultaneously; that is, no dewetting transition was observed.⁴⁶

To investigate further this fascinating dewetting phenomenon as well as its controlling factors during the amyloid fibrils formation, we use two β -sheets composed of hIAPP_{22–27} peptide (NFGAIL),^{23,24} a hydrophobic peptide whose aggregates are related to the type II diabetes,^{30,47,48} as the model system in this study. We have designed two different packing modes for the NFGAIL β -sheets (see Computational Models and Methods section for details) to mimic different confinement environment, one slab-like (2-D) and one tube-like (1-D). (See Figure 1.) For both packing modes, we observe water drying transitions in the confined region between two β -sheets, in which water expulsion precedes the hydrophobic collapse, but to our surprise, the 2-D like confinement has an even more profound dewetting transition than the 1-D like confinement. The kinetics of dewetting for two types of configurations are also quite different due to the different interfacial shapes. Moreover, we demonstrate the dramatic influence of internal surface topology of β -sheets pairs on the dewetting phenomenon through single mutations of the NFGAIL peptide. This study highlights the important role of packing modes (i.e., hydrophobic surface matching) in the assembly process of β -sheets and provides a deeper molecular understanding of the nanoscale dewetting during the self-assembly of amyloidogenic β -sheets. In addition, the present study suggests that the process of self-assembly of β -sheets can be regulated through mutations of the peptides on the β -sheets, which may have significance in practical applications.

COMPUTATIONAL MODELS AND METHODS

Both parallel and antiparallel β -sheets have been proposed for the hIAPP_{22–27} peptide fibril ladders in experiments,^{23,24} and the exact structures might depend on different initial seedings. In our current study, we adopted the antiparallel β -sheet conformation to build our model system, which consists of two relatively stable, flat, antiparallel β -sheets, with each sheet composed of eight antiparallel hIAPP_{22–27} (Ac–N²²–F²³–G²⁴–A²⁵–I²⁶–L²⁷–NH₂) peptides. The interpeptide separation, defined as the distance between the center of mass (COM) of two adjacent peptides, was set to be 0.47 nm,^{23,24,38,39} and the intersheet separation, D , defined as the distance between the COM of two β -sheets (as shown in Figure 1), is a variable in the current simulations. Following a similar approach as our previous study on the dewetting of $A\beta_{16–22}$ peptides,²¹ the two β -sheets were initially placed in two different conformations, classified by their packing modes of the internal-facing side chains: an “aligned” mode, with the side chains of one sheet aligned with the side chains of the other sheet (see Figure 1a,b, and Figure S1b in the Supporting

Information (SI) for details), forming a tube-like nanoscale channel (1-D like) (with an initial separation of 1.2 nm, the channel diameter is approximately equal to three water-molecule sizes), and a “staggered” mode (or steric-zipper-like), where the two facing sheets are laterally translated by a distance of 6 Å (see Figure 1 c,d, and Figure S1c in the SI for details), forming a zigzag slab-like confined space (2-D like). Hereafter we refer to the systems packing with the above two modes as “aligned”-type system and “staggered”-type system, respectively. For the “aligned”-type system, the nanochannel is enclosed by two kinds of hydrophobic residues (F²³ and A²⁵), together with the hydrophilic backbones of G²⁴ residues, whereas for the “staggered”-type system, the internal surface of protofilament is formed by the side chains of the three kinds of hydrophobic residues (F²³, A²⁵, and L²⁷) on the peptides together with the hydrophilic backbones of G²⁴ residues. For comparison, we also build an “A25I mutant system” based on a single mutation of Ala to Ile on each peptide of the “aligned”-type system. (See Figure 5 and its related discussions.)

All types of (8 × 2)-β-sheet protofilaments were then solvated in simple point charge (SPC) water⁴⁹ boxes with a minimum distance between the peptides and the edge of the box at least 1.2 nm. The solvated systems were simulated with MD, which is widely used in the studies of biomolecules,^{5,22,50–57} and nanoscale systems.^{58–60} The GROMACS 3.3.1 package was used,⁶¹ with the VMD software⁶² to view the trajectories and draw molecular pictures. The OPLSAA⁶³ force field was used for the NFGAIL/NFGIIL peptides. The particle-mesh Ewald method⁶⁴ was applied to treat the long-range electrostatic interactions, and a typical cutoff 10 Å was used for the van der Waals interactions. The LINCS algorithm⁶⁵ was used to constrain bond lengths within the solute, whereas the SETTLE algorithm⁶⁶ was used to constrain the bond lengths and angle in water. A time step of 2 fs was used for all simulations. The equilibration procedure starts with a 2000-step conjugate gradient minimization. After that, a 100 ps NVT relaxation procedure was performed to equilibrate the solvated systems, with the peptides atom positions restrained. Then, the production MD simulations were performed with an NPT ensemble (at 300 K and 1 atm, both constant temperature and constant pressure are controlled by the Berendsen methods,⁶⁷ with a coupling constant of 0.2 ps for thermostat and 20 ps for barostat), with initial configurations extracted from the NVT relaxation trajectories.

RESULTS AND DISCUSSIONS

For systems with both “aligned” and “staggered” packing modes, three different types of MD simulations were performed following a previous study:⁵ a “dewetting” simulation starting with wet initial conditions (the intersheet region filled with water molecules); a “wetting” simulation starting with dry initial conditions (no water molecule in the intersheet region); and a normal “assembly” simulation (all atoms in the system are free to move). In both the dewetting and wetting simulations, the positions of all heavy atoms on peptides are constrained by a harmonic potential with a spring constant of 1000 kJ mol⁻¹ nm⁻². The main purpose of “dewetting” and “wetting” simulations in the present study is to determine an approximate value of the dewetting critical distance, D_c .^{5,15,21} When the intersheet separation is less than D_c , water molecules will be expelled from the interior of the two positionally restrained sheets in a dewetting simulation and the interior region will remain dry in a wetting simulation. At

separations greater than D_c , the interior will remain hydrated in a dewetting simulation and become hydrated in a wetting simulation. At D_c , a dry interior should fluctuate between the wet and dry states with a large free energy barrier separating these states. If the barrier is sufficiently large, then a dry interior should remain dry and a solvated interior should remain wet during a finite time (the so-called hysteresis^{5,15}). To observe collapse for the “assembly” simulation on a relatively short time scale, we desire to set a not-too-large initial intersheet separation distance. In this study, we set it to be slightly larger than D_c once we identify the critical distance (more below).

Wetting and Dewetting Simulations. Figure 2a shows water density in the intersheet region during the course of aforementioned “dewetting” and “wetting” simulations (constrained simulations) for the “staggered”-type (2-D slab-like interface region) systems at different separation distances, D . For the “dewetting” simulations, we start from a larger separation distance, $D = 1.3$ nm, and then gradually reduce it to a smaller value of 0.9 nm. When D is relatively large, such as >1.0 nm, the initially trapped water molecules rarely escape from the intersheet region, but when D is reduced to 0.9 nm, nearly 70% of water molecules initially in the intersheet region are expelled but not completely exhausted yet. For the “wetting” simulations, we start from a smaller separation distance $D = 0.9$ nm and then gradually increase it to a larger value of 1.3 nm. When D is small such as 0.9 or 1.0 nm, very few water molecules can penetrate into the initially dry interior; when D is increased to 1.1 nm, more water molecules penetrate but are not completely wet yet. Only when D is above 1.2 nm the intersheet region becomes fully hydrated. Both the “dewetting” and “wetting” simulations indicate a critical distance of $D_c \approx 1.0$ to 1.1 nm. However, in the case of the “aligned”-type systems (1-D tube-like channel, Figure 2b), it is interesting to find that even if the intersheet separation is set to 0.7 nm, the initially dry interface can still get fully hydrated, which indicates that there is no D_c for this tightly constrained “aligned”-type system. It is generally accepted that the higher the confinement for water (such as lower dimensionality), the stronger the dewetting transition. Here, however, we observe that the 1-D like channel system has less dewetting than the 2-D-like slab system (more discussions below). A closer look indicates that the difference between two types of systems results from the steric effect of matching surfaces because there is a well-defined nanoscale channel in the central region (enclosed by F and A residues) with a relatively smooth internal surface for the “aligned”-type (1-D) system, although narrow, still capable of accommodating a few water molecules. In contrast, for the “staggered”-type (2-D) system, the tightly constrained side chains of F and L residues protrude into the interface of the two peptide sheets, forming a rough internal surface and thus are less capable of accommodating water molecules when D decreases to a small value. In the following “assembly” simulations, we will observe once the local side chains of the 1-D like tube system are also allowed to move freely that the matching surfaces will become rough, which will squeeze water molecules out, resulting in dewetting transition in 1-D like tube as well (although still somewhat weaker than the 2-D slab system).

Assembly Simulations. Next, we have performed the “assembly” simulation (unconstrained simulations) for both the “aligned”- and “staggered”-type systems starting at the same initial separation of 1.2 nm, which is slightly larger than the critical distance for “staggered” system, with 10 independent runs for each type system to study the dynamics of the collapsing process.

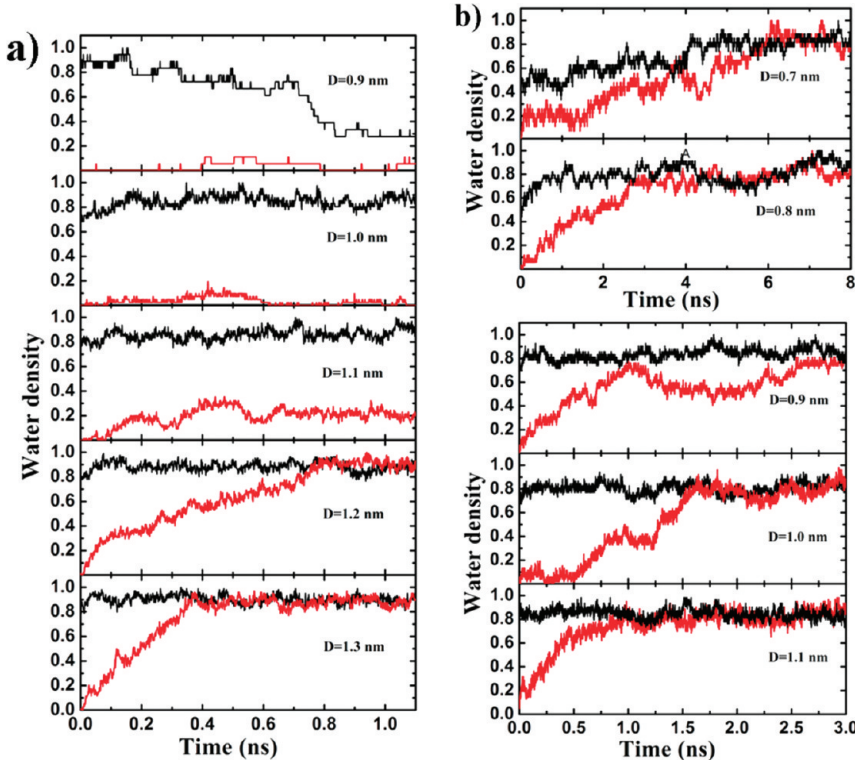


Figure 2. Water density in the intersheet region as the function of time for five different intersheet separations, D , for “staggered”-type (2-D slab-like interface region) system (a) and “aligned”-type (1-D tube-like channel) system (b), respectively. The red curves stand for the “wetting” simulations, whereas the black curves stand for the “dewetting” simulations. Different time scales are used for various subfigures to illustrate the changes in the water density with time better.

In all trajectories, despite different initial packing arrangements, we observe that both “aligned”- and “staggered”-type systems spontaneously assemble into protofilaments with somewhat of a twist of the β -sheets, accompanied by expelling nearly all water molecules out of the intersheet region; eventually, most of the facing side chains of the two β -sheets interdigitate, forming a dry interface. (See Figure 3.) During this assembly process, the channel-like and slab-like interfaces for the “aligned”- and “staggered”-type systems are largely maintained, respectively (see Figure 3), and the initial 6 Å lateral shift is also largely intact in the final structure of the “staggered” packing mode system. This means the initial packing mode is important for the dewetting and assembly of the amyloid β -sheets in the formation of fibrils, and the final adjustments of these packing sheets can take much more time, which is beyond our current simulation lengths. These representative snapshots of self-assembly processes provide a general route for the lateral formation of protofilament. Compared with the results of “assembly” simulation, the apparent lack of depletion of water for the constrained simulations of “aligned”-type systems may be due to the fact that the side chains of the β -sheets are constrained to a fixed packing geometry, which lacks the freedom to interact with water and form optimal geometry to “squeeze” water out. This viewpoint can be further validated by the “partly constrained” simulation, during which all atoms of the side chains are free to move with only α carbon atoms constrained. Figure S2 of the Supporting Information shows that for “partly constrained” simulation of “aligned”-type system, even if the separation distance D is as large as 1.0 nm, the initial wet interior gradually becomes dry, in contrast with the above result that there is no dewetting transition for “aligned”-type system even when $D = 0.7$ nm, if all heavy atoms

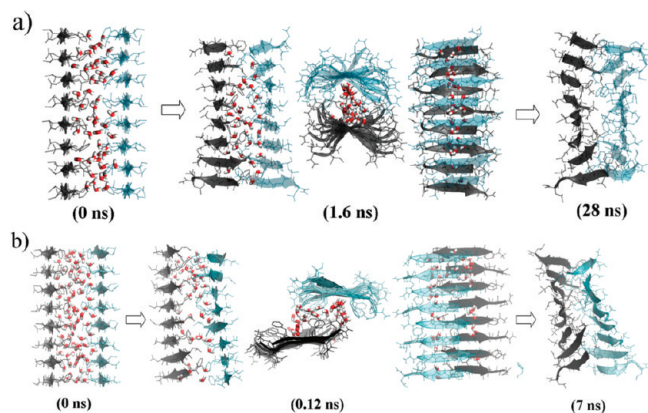


Figure 3. A few representative snapshots from assembly simulations of the (a) “aligned”- and (b) “staggered”-type systems, with initial intersheet separation D of 1.2 nm. The typical intermediate states in the self-assembly processes (1.6 ns for “aligned”-type system, 0.12 ns for “staggered”-type system) are depicted from side view (left), longitudinal view (middle), and lateral view (right). The NFGAIL peptide sheet is shown as ribbons with side chains in sticks, and water is shown as thick bonds.

on peptides are constrained, indicating the local side-chain packing is very important in the final squeezing of water molecules because of the strong hydrophobic force.

The molecular picture of β -sheets assembly is quantified through plotting the number of water molecules in the intersheet region and the intersheet distance with respect to simulation time. Some representative ones are shown in top panels of

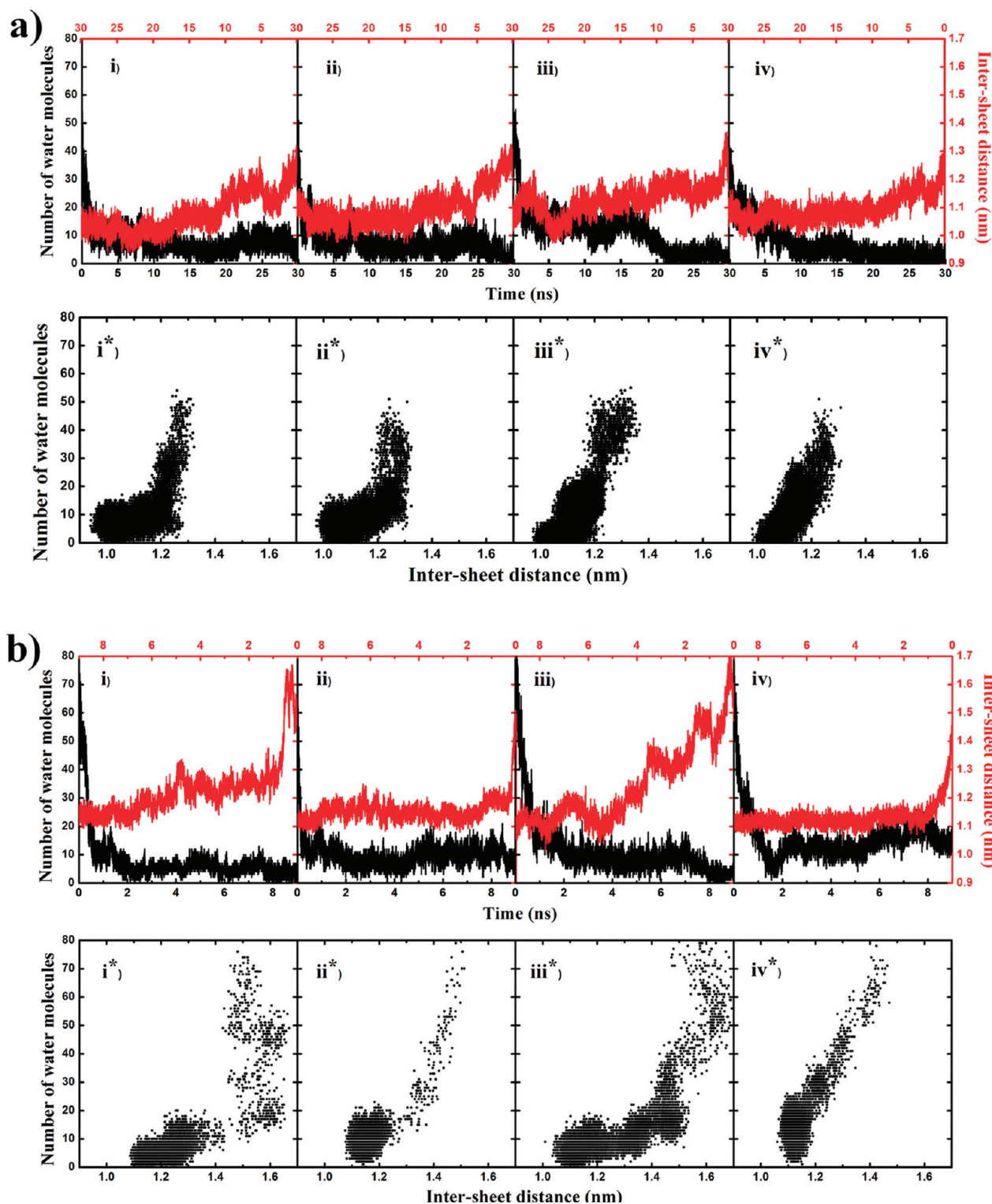


Figure 4. Some representative trajectories to show the kinetics of dewetting and collapse of β -sheets pairs for the “assembly” simulations starting at $D = 1.2$ nm. (a, top) Number of water molecules (black) in the intersheet region and the intersheet distance (red) as a function of simulation time for “aligned”-type system. Each plot shows a different trajectory. The time scales for the number of water molecules (black) and the intersheet distance (red) are drawn in opposite directions for a better illustration of these trajectories (otherwise, the two curves will be overlapping). (a, bottom) Water numbers in the intersheet region versus intersheet distance for “aligned”-type system. (Each plot corresponds to the same trajectory as the plot above it.) (b) Same as part a but from the simulations for “staggered”-type system. Trajectories of i* and ii* in (a) and i*-iii* in (b) show dewetting transitions, whereas other trajectories do not.

Figure 4a,b. Dramatic decreases in the number of water molecules are observed in a few nanoseconds in all trajectories;

however, the time scale of collapse of two β -sheets can take up to ~ 20 ns (Figure 4a). To explore further the role of water in

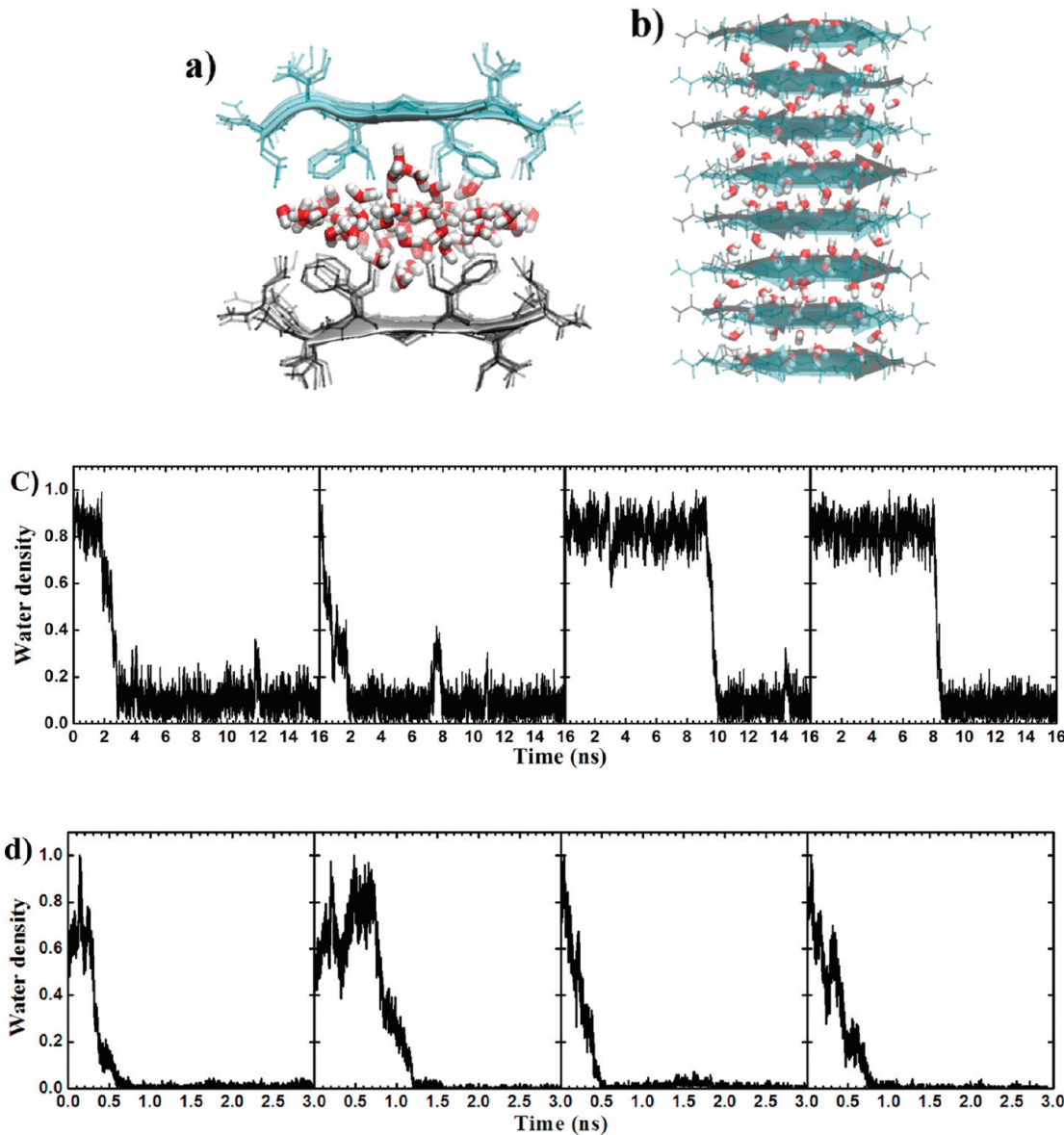


Figure 5. Simulations of the A2SI mutant system starting at the initial intersheet separation of $D = 1.4$ nm. (a,b) Snapshots of initial configurations of the systems in longitudinal (a) and lateral (b), respectively. (c,d) “Dewetting” simulations (with peptides atoms constrained) (c) and “Assembly” simulations (d) for the A2SI mutant system, with the water density shown as a function of simulation time. Each plot shows a different trajectory.

the β -sheets collapse, we plot the number of water molecules in the intersheet region against the intersheet distance, as shown in bottom panels of Figure 4a,b. In some trajectories (i* and ii* in Figure 4a and i*-iii* in Figure 4b), we observe a dramatic decrease in the number of water molecules, followed by a decrease in the intersheet distance. These results indicate that a dewetting transition can occur in the intersheet region for both “aligned”- and “staggered”-type systems, and this in turn provides large driving forces to push the two β -sheets together, as previously observed in simulations of the collapse of paraffin-like plates where the collapse was found to be rate-limited by the nucleation of a vapor bubble in the gap,¹⁵ whereas in some other trajectories (iii* and iv* in Figure 4a and iv* in Figure 4b) the collapse of the two sheets and expulsion of water molecules appear to occur nearly simultaneously. Through energetic analyses for these trajectories, we find that these kinds of protofilament self-assembly are driven by direct interactions between

internal-facing side chains of peptides with the residue pairs F–F, and F–L interactions contributed most. (See Figure S3 in the SI.)

To characterize quantitatively the dynamics of β -sheets assembly process and facilitate direct comparison between “aligned”- and “staggered”-type systems, we have calculated the duration time of water depletion process, together with the occurrence probability of dewetting transition, for all “assembly” simulations. This duration time is defined as the simulation time needed for “exhausting” water. (In some cases, although dewetting processes have finished, there are still a few water molecules remaining in the interior of the protofilament (commonly at the edge of the protofilament), so we define the starting time as that when the number of water molecules starts to decrease monotonously and sharply and the end time as that when it starts to converge.) In the case of “aligned”-type (1-D) systems, dewetting transitions are observed in 5 out of 10 trajectories, and the

average duration time of water depletion (denoted by $\langle T \rangle$) is 12.6 ± 7.6 ns, whereas in the case of “staggered”-type simulations, an even higher occurrence possibility of dewetting transition (7 out of 10 trajectories) and a much faster process for water depletion ($\langle T \rangle = 2.8 \pm 1.8$ ns) are observed. The results of both the occurrence possibility and time scale for water depletion indicate that the “staggered”-type system shows stronger dewetting phenomenon than the “aligned”-type system. In general, 1-D confined space (i.e., a tube-like channel) shows stronger dewetting phenomenon than the 2-D (i.e., a slab-like) confined space because it is less costly in terms of free energy to disrupt the hydrogen bonds in a tube-like channel. The present simulation results are somewhat unexpected because of the stronger dewetting phenomenon observed for the “staggered” packing mode (2-D); that is, the “2-D dewetting” is stronger than “1-D dewetting” in this case. This indicates that the matching hydrophobic surface topology (roughness) can have profound influence on the dewetting phenomenon. The stronger dewetting phenomenon observed here is due to the fact that the rough matching surfaces for the “staggered” packing mode disrupt more on the water hydrogen bond network than the relatively smoother surfaces in the 1-D-like tube for the “aligned” packing mode. Consequently, we have demonstrated that the initial packing mode of β -sheets can influence the surface topology of intersheet region and in turn profoundly influence the assembly (and dewetting) process of β -sheets. Also note that the time scale for dewetting and collapse of two β -sheets of hIAPP_{22–27} peptides ranges from ~ 1 to ~ 20 ns, which is orders of magnitude slower than those for two A β _{16–22} peptides β -sheets (in which case dry transition occurs ~ 200 ps)²¹ and is comparable to those for two A β _{37–42} peptides β -sheets (a few nanoseconds).⁴⁶ Accordingly, apart from the packing modes, there are some other factors determining the assembly (dewetting) processes, such as sizes and surface hydrophobicity of the intersheet regions.

Mutant Simulations. To explore further the influence of surface hydrophobicity and topology on the kinetics of dewetting, we have designed a model system, namely, “A25I mutant system” (NFGAIL protofilament), based on a single mutation Ala25 residue being replaced by Ile25. Compared with Ala residue, Ile residue is more hydrophobic because of a longer hydrophobic side chain. Therefore, we expect a more profound dewetting phenomenon for the A25I mutant systems. We have performed a set of 16 ns “dewetting” simulations (with all heavy atoms of peptides constrained) to study this single mutation effect using the “aligned” packing system (1-D) as an example. Remember in the above “dewetting” simulations that there is no dewetting critical distance for the wild-type “aligned” system, even if the intersheet separation is set to $D = 0.7$ nm. Figure 5 shows the results for this mutant “aligned” system. Remarkably, we observe strong liquid–vapor transitions even at $D = 1.4$ nm (Figure 5c), which is significantly larger than that of wild-type “aligned”-type system (no dewetting even at a smaller distance of 0.7 nm (see Figure 2b)). In addition, the “assembly” simulations (Figure 5d) also show dewetting transitions, much more profound, with the average time needed for water depletion in these mutant “assembly” simulations only 0.7 ± 0.1 ns, which is more than one order of magnitude faster than that of the wild-type “aligned” system (12.6 ± 7.6 ns). We rationalize this drying phenomenon as follows: compared with the wildtype “aligned”-type system, the residues of Ala are replaced by Ile residues with longer hydrophobic side chains. These long side chains protrude

from the sidewall of β -sheets, acting as “surface bumps” (making very rough surfaces), disrupting the hydrogen-bond network of water that originally situated in the confined region and thus making the wet configurations less favorable.²² The above simulation results for the A25I mutant systems strongly suggest that the surface topology can profoundly influence the dewetting process in the protofilament formation. These results also suggest that the speed of self-assembly process can be controllably regulated through mutations of the peptides on the β -sheets. As mentioned in the Introduction, the amyloid fibrils can be promising materials for many technological applications; therefore, these findings may have significance in practical applications.

CONCLUSIONS

In this study, we perform MD simulations of the self-assembly of two amyloidogenic β -sheets of hIAPP_{22–27} peptides (NFGAIL) that are mediated by water. The initial configurations of two β -sheets are arranged in an “aligned” packing mode, enclosing a one-dimensionally channel-like region with a size of approximately two to three water-molecule diameters and a “staggered” packing mode, forming a two-dimensionally confined space with a slab-like water layer. For both packing modes, we observe strong water drying transitions in the intersheet region with high occurrence possibilities, suggesting that the “drying transition”-induced collapse may play an important role in promoting the formation of protofilaments. Interestingly, the “staggered”-type (2-D) system shows stronger dewetting phenomenon than the “aligned” system (1-D). This observation is unexpected because the tube-like confined space (“aligned”-type system) usually shows stronger dewetting phenomenon than the slab-like confined space (“staggered”-type system) based on general dewetting theory prediction. We attribute this unexpected phenomenon to the different matching surface roughness caused by different packing modes. In addition, we demonstrate the profound influence of matching surface topology of β -sheet pairs on the dewetting phenomenon through a mutation study. This study highlights the important role of packing modes (i.e., matching surface roughness) in the assembly process of β -sheets and improves our understanding toward the molecular mechanism underlying protofilaments formation as well as nanoscale dewetting phenomenon. Moreover, our study also suggests a potential route to regulate controllably the self-assembly process of β -sheets through mutations of the peptides on the β -sheets, which may have important applications in nanotechnology and biotechnology.

ASSOCIATED CONTENT

S Supporting Information. Detailed description of two packing modes of β -sheets pairs, dewetting transition in “partly constrained” simulation of “aligned”-type system at $D = 1.0$ nm, and an energetic analysis of the driving force for protofilament self-assembly. This material is available free of charge via the Internet at <http://pubs.acs.org>.

AUTHOR INFORMATION

Corresponding Author

*E-mail: xiupeng2011@zju.edu.cn (P.X.), ruhongz@us.ibm.com (R.Z.).

■ ACKNOWLEDGMENT

We thank Xiaowei Tang, Yuanyuan Qu, Xiongfei Fu, and Bruce J. Berne for helpful discussions and comments. This work is partially supported by the National Natural Science Foundation of China (grant nos. 30870593 and 11005093), the Zhejiang Provincial Natural Science Foundation (grant no. Y6100384), and the Fundamental Research Funds for the Central Universities. R.Z. acknowledges the support from the IBM BlueGene Program.

■ REFERENCES

- (1) Dobson, C. M.; Sali, A.; Karplus, M. *Angew. Chem., Int. Ed.* **1998**, *37*, 868.
- (2) Socci, N. D.; Onuchic, J. N.; Wolynes, P. G. *Proteins: Struct., Funct., Genet.* **1998**, *32*, 136.
- (3) Dill, K. A.; Chan, H. S. *Nat. Struct. Biol.* **1997**, *4*, 10.
- (4) Brooks, C. L.; Gruebele, M.; Onuchic, J. N.; Wolynes, P. G. *Proc. Natl. Acad. Sci. U.S.A.* **1998**, *95*, 11037.
- (5) Zhou, R. H.; Huang, X. H.; Margulis, C. J.; Berne, B. J. *Science* **2004**, *305*, 1605.
- (6) Hua, L.; Huang, X. H.; Liu, P.; Zhou, R. H.; Berne, B. J. *J. Phys. Chem. B* **2007**, *111*, 9069.
- (7) Young, T.; Hua, L.; Huang, X. H.; Abel, R.; Friesner, R.; Berne, B. J. *Proteins: Struct., Funct., Genet.* **2010**, *78*, 1856.
- (8) Abel, R.; Young, T.; Farid, R.; Berne, B. J.; Friesner, R. A. *J. Am. Chem. Soc.* **2008**, *130*, 2817.
- (9) Friesner, R. A.; Murphy, R. B.; Repasky, M. P.; Frye, L. L.; Greenwood, J. R.; Halgren, T. A.; Sanschagrin, P. C.; Mainz, D. T. *J. Med. Chem.* **2006**, *49*, 6177.
- (10) Tanford, C. *J. Mol. Biol.* **1972**, *67*, 59.
- (11) Israelachvili, J. N.; Mitchell, D. J.; Ninham, B. W. *J. Chem. Soc., Faraday Trans. 2* **1976**, *72*, 1525.
- (12) Roth, R.; Gillespie, D.; Nonner, W.; Eisenberg, R. E. *Biophys. J.* **2008**, *94*, 4282.
- (13) Anishkin, A.; Sukharev, S. *Biophys. J.* **2004**, *86*, 2883.
- (14) Lum, K.; Chandler, D.; Weeks, J. D. *J. Phys. Chem. B* **1999**, *103*, 4570.
- (15) Huang, X.; Margulis, C. J.; Berne, B. J. *Proc. Natl. Acad. Sci. U.S.A.* **2003**, *100*, 11953.
- (16) ten Wolde, P. R.; Chandler, D. *Proc. Natl. Acad. Sci. U.S.A.* **2002**, *99*, 6539.
- (17) Li, X.; Li, J. Y.; Eleftheriou, M.; Zhou, R. H. *J. Am. Chem. Soc.* **2006**, *128*, 12439.
- (18) Hua, L.; Zangi, R.; Berne, B. J. *J. Phys. Chem. C* **2009**, *113*, 5244.
- (19) Hummer, G.; Rasaiah, J. C.; Noworyta, J. P. *Nature* **2001**, *414*, 188.
- (20) Berne, B. J.; Weeks, J. D.; Zhou, R. H. *Annu. Rev. Phys. Chem.* **2009**, *60*, 85.
- (21) Krone, M. G.; Hua, L.; Soto, P.; Zhou, R. H.; Berne, B. J.; Shea, J. E. *J. Am. Chem. Soc.* **2008**, *130*, 11066.
- (22) Liu, P.; Huang, X. H.; Zhou, R. H.; Berne, B. J. *Nature* **2005**, *437*, 159.
- (23) Madine, J.; Jack, E.; Stockley, P. G.; Radford, S. E.; Serpell, L. C.; Middleton, D. A. *J. Am. Chem. Soc.* **2008**, *130*, 14990.
- (24) Nielsen, J. T.; Bjerring, M.; Jeppesen, M. D.; Pedersen, R. O.; Pedersen, J. M.; Hein, K. L.; Vosegaard, T.; Skrydstrup, T.; Otzen, D. E.; Nielsen, N. C. *Angew. Chem., Int. Ed.* **2009**, *48*, 2118.
- (25) Chiti, F.; Dobson, C. M. *Annu. Rev. Biochem.* **2006**, *75*, 333.
- (26) Murphy, R. M. *Annu. Rev. Biomed. Eng.* **2002**, *4*, 155.
- (27) Hardy, J.; Selkoe, D. J. *Science* **2002**, *297*, 353.
- (28) Selkoe, D. J. *Nature* **2003**, *426*, 900.
- (29) Wu, C.; Lei, H. X.; Duan, Y. *Biophys. J.* **2004**, *87*, 3000.
- (30) Höppener, J. W. M.; Ahren, B.; Lips, C. J. M. N. *Engl. J. Med.* **2000**, *343*, 411.
- (31) Thirumalai, D.; Klimov, D. K.; Dima, R. I. *Curr. Opin. Struct. Biol.* **2003**, *13*, 146.
- (32) Dobson, C. M. *Nature* **2003**, *426*, 884.
- (33) Kayed, R.; Head, E.; Thompson, J. L.; McIntire, T. M.; Milton, S. C.; Cotman, C. W.; Glabe, C. G. *Science* **2003**, *300*, 486.
- (34) Gras, S. L. *Aust. J. Chem.* **2007**, *60*, 333.
- (35) Hamada, D.; Yanagihara, I.; Tsumoto, K. *Trends Biotechnol.* **2004**, *22*, 93.
- (36) Rajagopal, K.; Schneider, J. P. *Curr. Opin. Struct. Biol.* **2004**, *14*, 480.
- (37) Zhang, S. G. *Nat. Biotechnol.* **2003**, *21*, 1171.
- (38) Sawaya, M. R.; Sambashivan, S.; Nelson, R.; Ivanova, M. I.; Sievers, S. A.; Apostol, M. I.; Thompson, M. J.; Balbirnie, M.; Wiltzius, J. J. W.; McFarlane, H. T.; Madsen, A. O.; Riekel, C.; Eisenberg, D. *Nature* **2007**, *447*, 453.
- (39) Nelson, R.; Sawaya, M. R.; Balbirnie, M.; Madsen, A. O.; Riekel, C.; Grothe, R.; Eisenberg, D. *Nature* **2005**, *435*, 773.
- (40) Toyama, B. H.; Kelly, M. J. S.; Gross, J. D.; Weissman, J. S. *Nature* **2007**, *449*, 233.
- (41) van der Wel, P. C. A.; Lowandowski, J. R.; Griffin, R. G. *Biochemistry* **2010**, *49*, 9457.
- (42) Esposito, L.; Pedone, C.; Vitagliano, L. *Proc. Natl. Acad. Sci. U.S.A.* **2006**, *103*, 11533.
- (43) Tseng, B. P.; Esler, W. P.; Clish, C. B.; Stimson, E. R.; Ghilardi, J. R.; Vinters, H. V.; Mantyh, P. W.; Lee, J. P.; Maggio, J. E. *Biochemistry* **1999**, *38*, 10424.
- (44) Nichols, M. R.; Moss, M. A.; Reed, D. K.; Lin, W. L.; Mukhopadhyay, R.; Hoh, J. H.; Rosenberry, T. L. *Biochemistry* **2002**, *41*, 6115.
- (45) Green, J. D.; Goldsbury, C.; Kistler, J.; Cooper, G. J. S.; Aebi, U. *J. Biol. Chem.* **2004**, *279*, 12206.
- (46) Reddy, G.; Straub, J. E.; Thirumalai, D. *Proc. Natl. Acad. Sci. U.S.A.* **2010**, *107*, 21459.
- (47) Westermark, P.; Wernstedt, C.; Obrien, T. D.; Hayden, D. W.; Johnson, K. H. *Am. J. Pathol.* **1987**, *127*, 414.
- (48) Lorenzo, A.; Razzaboni, B.; Weir, G. C.; Yankner, B. A. *Nature* **1994**, *368*, 756.
- (49) Berendsen, H. J. C.; Postma, J. P. M.; van Gunsteren, W. F.; Hermans, J. *Intermolecular Forces*; Reidel: Dordrecht, The Netherlands, 1981; p 331.
- (50) Duan, Y.; Kollman, P. A. *Science* **1998**, *282*, 740.
- (51) Snow, C. D.; Nguyen, N.; Pande, V. S.; Gruebele, M. *Nature* **2002**, *420*, 102.
- (52) Garcia, A. E.; Paschek, D. *J. Am. Chem. Soc.* **2008**, *130*, 815.
- (53) Zhou, R. H.; Eleftheriou, M.; Royyuru, A. K.; Berne, B. J. *Proc. Natl. Acad. Sci. U.S.A.* **2007**, *104*, 5824.
- (54) Karplus, M.; Gao, Y. Q.; Ma, J.; van der Vaart, A.; Yang, W. *Philos. Trans. R. Soc., A* **2005**, *363*, 331.
- (55) Zhou, R.; Berne, B. J.; Germain, R. *Proc. Natl. Acad. Sci. U.S.A.* **2001**, *98*, 14931.
- (56) Eleftheriou, M.; Germain, R. S.; Royyuru, A. K.; Zhou, R. *J. Am. Chem. Soc.* **2006**, *128*, 13388.
- (57) Hua, L.; Huang, X.; Liu, P.; Zhou, R.; Berne, B. J. *J. Phys. Chem. B* **2007**, *111*, 9069.
- (58) Hummer, G.; Rasaiah, J. C.; Noworyta, J. P. *Nature* **2001**, *414*, 188.
- (59) Tu, Y. S.; Xiu, P.; Wan, R. Z.; Hu, J.; Zhou, R. H.; Fang, H. P. *Proc. Natl. Acad. Sci. U.S.A.* **2009**, *106*, 18120.
- (60) Tu, Y.; Zhou, R.; Fang, H. *Nanoscale* **2010**, *2*, 1976.
- (61) Lindahl, E.; Hess, B.; van der Spoel, D. *J. Mol. Model.* **2001**, *7*, 306.
- (62) Humphrey, W.; Dalke, A.; Schulten, K. *J. Mol. Graphics* **1996**, *14*, 33.
- (63) Jorgensen, W. L.; Maxwell, D. S.; TiradoRives, J. *J. Am. Chem. Soc.* **1996**, *118*, 11225.
- (64) Essmann, U.; Perera, L.; Berkowitz, M. L.; Darden, T.; Lee, H.; Pedersen, L. G. *J. Chem. Phys.* **1995**, *103*, 8577.
- (65) Hess, B.; Bekker, H.; Berendsen, H. J. C.; Fraaije, J. *J. Comput. Chem.* **1997**, *18*, 1463.
- (66) Miyamoto, S.; Kollman, P. A. *J. Comput. Chem.* **1992**, *13*, 952.
- (67) Berendsen, H. J. C.; Postma, J. P. M.; Vangunsteren, W. F.; Dinola, A.; Haak, J. R. *J. Chem. Phys.* **1984**, *81*, 3684.